Chemical Physics Letters 715 (2019) 134–140

Contents lists available at ScienceDirect

Chemical Physics Letters

journal homepage: www.elsevier.com/locate/cplett

Research paper

# Tuning the porosity of $TiO_2$ nanoparticles via surfactant-templated aerosol process for enhanced photocatalytic reactivity

Ji Hye Ku[a], Ho Sung Kim[a], Myung Hoon Cho[b], Ji Young Ahn[b], Soo Hyung Kim[a,b,c,*]

[a] Department of Nano Fusion Technology, College of Nanoscience and Nanotechnology, Pusan National University, 30 Jangjeon-dong, Geumjung-gu, Busan 609-735, Republic of Korea
[b] Research Center for Energy Convergence Technology, Pusan National University, 30 Jangjeon-dong, Geumjung-gu, Busan 609-735, Republic of Korea
[c] Department of Nanoenergy Engineering, College of Nanoscience and Nanotechnology, Pusan National University, 30 Jangjeon-dong, Geumjung-gu, Busan 609-735, Republic of Korea

## HIGHLIGHTS

- $TiO_2$ nanoparticles (NPs) with intra-particle porosity are fabricated using surfactant-tempted aerosol process.
- Surfactant plays the role as a templating medium to support pore structures inside $TiO_2$ matrix.
- $TiO_2$ NPs with highly porous structures enhance the photodegradation of methylene blue.

## ARTICLE INFO

*Keywords:*
Aerosol process
Porous $TiO_2$ nanoparticles
Photocatalysts
Surfactants
Specific surface area

## ABSTRACT

In this work, we fabricated crystallite solid and porous $TiO_2$ nanoparticles (NPs) using a surfactant-templated aerosol process. Specifically, Brij-58 surfactant was employed as a template in $TiO_2$ matrix. The porosity of $TiO_2$ NPs was controlled by varying the amount of Brij-58. The effect of $TiO_2$ porosity on the photocatalytic reactivity was systematically examined. As a result, the highly porous $TiO_2$ NPs exhibited much better photocatalytic reactivity than the low porosity $TiO_2$ NPs. This suggests that the particle size, crystallite structure, and specific surface area play an important role in enhancing the photocatalytic reactivity of the $TiO_2$ NPs.

## 1. Introduction

Among many semiconducting metal oxides, $TiO_2$ is known as a highly-valued material suitable for industrial applications, due to its many advantages such as relatively high chemical stability, nontoxicity, relatively low manufacturing cost, and highly oxidizing reactivity [1–8]. Since $TiO_2$ has a band gap of 3.0–3.2 eV, it can effectively absorb ultraviolet (UV) light. The mechanism of photocatalytic process of $TiO_2$ particles is generally known that an electron from the valence band (VB) promotes to the conduction band (CB), leaving an electron deficiency (h+) in the VB and an excess of negative charge (e-) in the CB, which are oxidizing and reducing equivalents and can participate in redox reactions when the light irradiates on the $TiO_2$ catalyst (Fig. 1). Moreover, $TiO_2$ nanoparticles (NPs) are known to have a superior photocatalytic reactivity compared to traditional bulk $TiO_2$. Thus, various approaches have been developed towards the synthesis of $TiO_2$ NPs. These include methods such as sol-gel [9], solvothermal [10], hydrothermal [11], direct oxidation [12], chemical vapor deposition (CVD) [13], electrospinning deposition [14–16], microwave [17], and spray pyrolysis [18]. From the aforementioned approaches, the spray pyrolysis method displays many advantages in that it can continuously and cost-effectively generate $TiO_2$ NPs with control on the structure [18–22].

The photocatalytic reactivity of $TiO_2$ NPs is strongly dependent on their structural characteristics as well as the synthetic methods employed [23]. Recently, mesoporous $TiO_2$ NPs with a relatively high specific surface area have been synthesized in a way that their photocatalytic performance is enhanced [24–26]. Mesoporous $TiO_2$ NPs have a high photocatalytic reactivity due to their porous structure, which can lead to an increase in the interfacial contact area between $TiO_2$ and pollutants [27]. In addition, these NPs are particularly important because of their good stability and ability to enhance light harvesting [28–31]. There have been numerous approaches that have been developed to synthesize the important NPs. One way to effectively create

* Corresponding author at: Department of Nanoenergy Engineering, College of Nanoscience and Nanotechnology, Pusan National University, 30 Jangjeon-dong, Geumjung-gu, Busan 609-735, Republic of Korea.
*E-mail address:* sookim@pusan.ac.kr (S.H. Kim).

https://doi.org/10.1016/j.cplett.2018.11.029
Received 26 September 2018; Received in revised form 6 November 2018; Accepted 13 November 2018
Available online 14 November 2018
0009-2614/ 

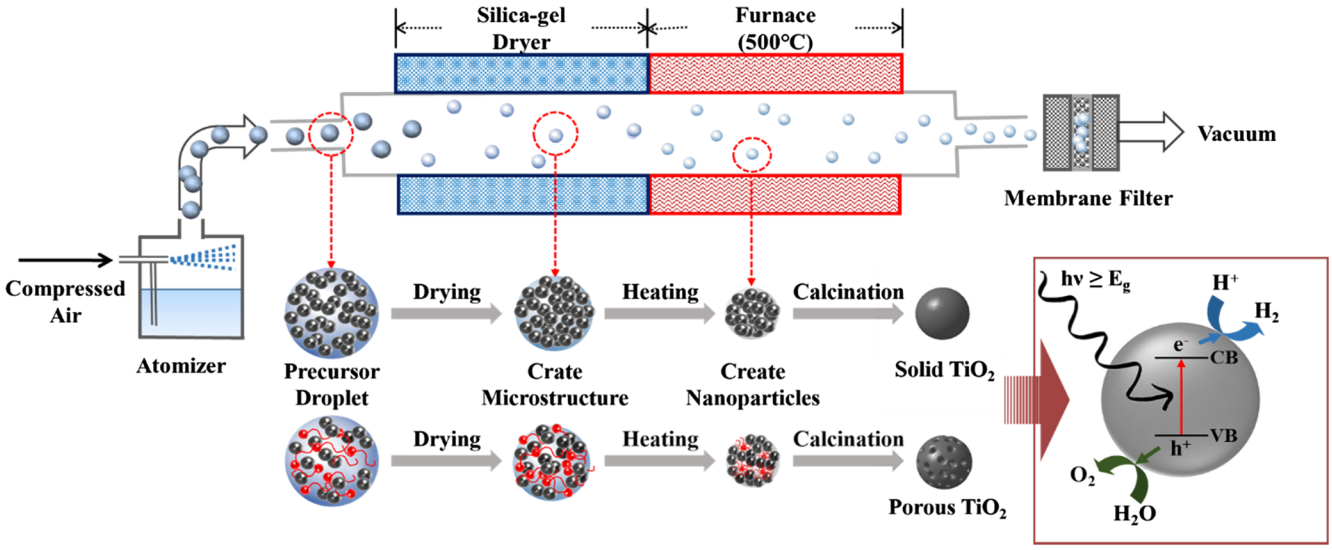


**Fig. 1.** Schematic of aerosol synthesis and photocatalytic process of surfactant-templated solid and porous $TiO_2$ particles.

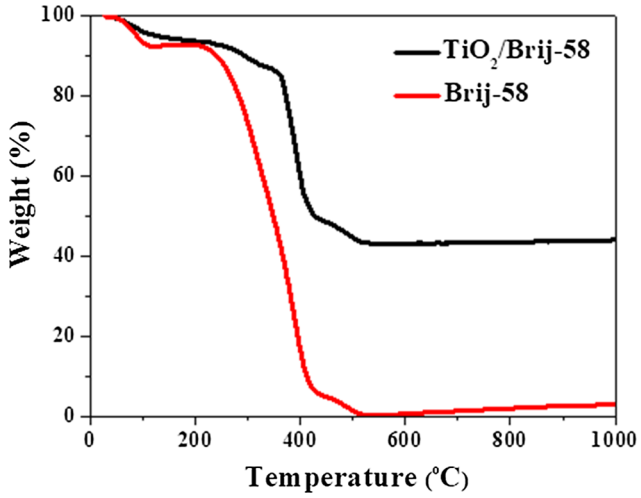


**Fig. 2.** Thermogravimetric analysis of Brij-58 (red) and Brij-58/$TiO_2$ (black) samples. (For interpretation of the references to colour in this figure legend, the reader is referred to the web version of this article.)

pore structures inside the $TiO_2$ matrix is to use a surfactant as templating medium [32,33]. After the surfactant templates are removed, the porosity of the resulting $TiO_2$ NPs is strongly dependent on the nature and initial concentration of the surfactant in the given synthetic method [32–37]. Several research groups reported the successful fabrication of mesoporous $TiO_2$ NPs, but they did not conduct a systematic exploration of the control and effect that $TiO_2$ porosity has on the photocatalytic performance.

In this work, we systematically investigated the use of Brij-58 as a nonionic surfactant template and its effect on the formation of porous structures inside the $TiO_2$ NPs. Both solid and porous $TiO_2$ NPs were fabricated using different mixing molar ratios of $TiO_2$ and Brij-58 in the aerosol process. The synthesized $TiO_2$ NPs were then systematically examined using various analytical techniques, including scanning electron microscope (SEM), transmission electron microscope (TEM), and nitrogen gas adsorption to identify the formation of porous structures in the $TiO_2$ matrix. Furthermore, the photocatalytic reactivity of the $TiO_2$ NPs was examined by testing the photodegradation of methylene blue (MB) solution in the presence of these NPs under different UV light irradiation durations.

## 2. Experimental

### 2.1. Fabrication of $TiO_2$ NPs

A $TiO_2$ precursor solution was prepared by mixing titanium butoxide (tetra-n-butyl orthotitanate [TNBT ($C_{16}H_{40}O_4Ti$); Sigma-Aldrich, St. Louis, MO, USA], deionized water, and ethanol. TNBT (17.15 ml) was initially dissolved in ethanol (72.85 ml). Deionized water (90 ml) was then gradually added to the solution under continuous stirring, which resulted in the rapid precipitation of $TiO_2$. In order to fabricate porous $TiO_2$ NPs, nonionic surfactant [Brij-58; $CH_3(CH_2)_{15}$-$(OCH_2CH_2)_{20}$-OH; Sigma-Aldrich, St. Louis, MO, USA] was used as an organic template and added in the $TiO_2$ solution. The initial concentration of Brij-58 was varied from 0.0 to 0.1 M. HCl was then added to adjust the pH of $TiO_2$ solution. The final molar ratio was determined to be TNBT:$H_2O$:HCl:Brij-58 = 1:67:0.004:(0.0–0.1). The aforementioned sol-gel-chemistry-generated $TiO_2$ precursor solution was first aerosolized using a standard atomizer with compressed air at a pressure of 35 kN $m^{-2}$ as shown in Fig. 1. The aerosol droplets were then rapidly solidified due to the solvent evaporation that occurred when they passed through a silica-gel dryer. The dried aerosol particles were then continuously passed through a quartz tube (2.54 cm in diameter × 40 cm in heating length) enclosed with a heating reactor at ~500 °C. Finally, the $TiO_2$ particles were collected on a membrane filter with an average pore size of ~200 nm, and then additionally heated at ~550 °C for 1 h in a convection oven to thermally remove the Brij-58 surfactants and any residues.

### 2.2. Characterization of $TiO_2$ NPs

XRD (Empyrean series 2, PANalytical, Almero, Netherlands) with Cu Kα radiation was used to examine the crystallinity of the $TiO_2$ NPs fabricated in this study. The size and morphology of the resulting solid and porous $TiO_2$ NPs were measured using a SEM (S-4200, Hitachi, Tokyo, Japan) operated at ~15 kV and TEM (JEM 2100F, JEOL, Tokyo,

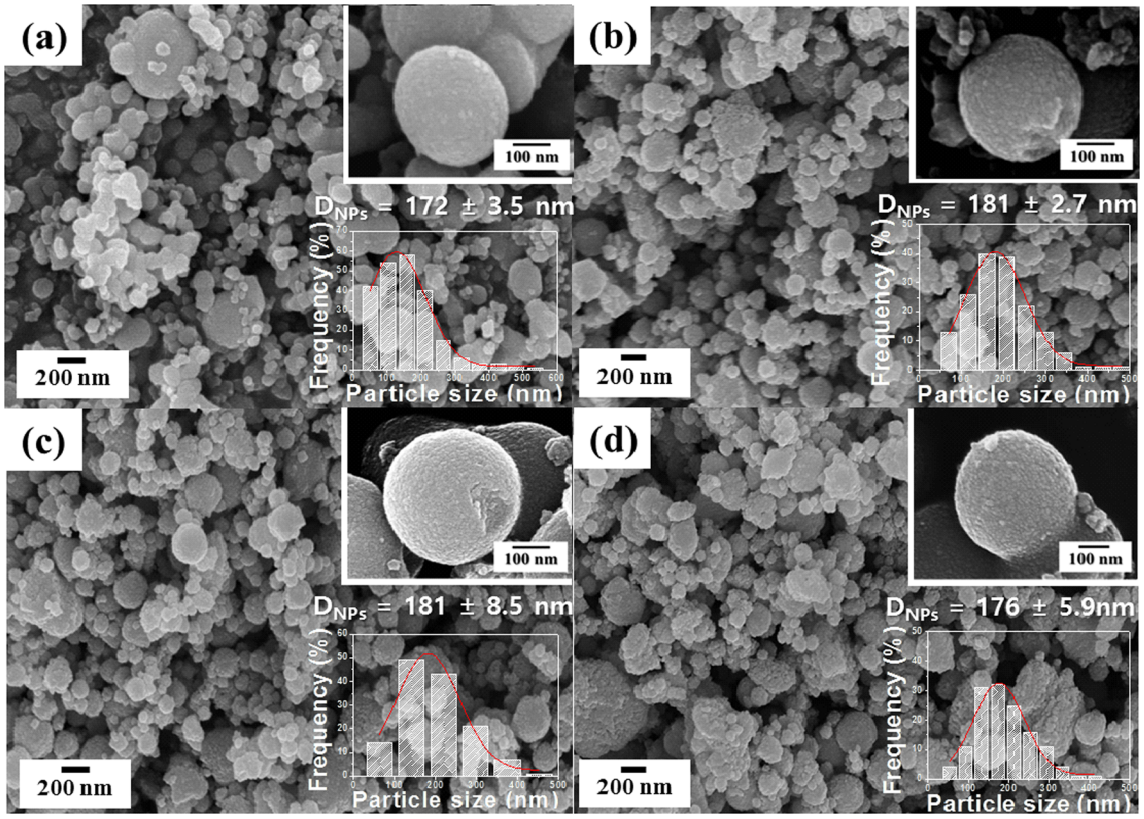


**Fig. 3.** FE-SEM images of $TiO_2$ NPs made by various mixing ratios: (a) TNBT:Brij-58 = 1:0.00, (b) TNBT:Brij-58 = 1:0.01, (c) TNBT:Brij-58 = 1:0.05, and (d) TNBT:Brij-58 = 1:0.10. (Insets are HR-SEM images of the $TiO_2$ NPs. $D_{NPs}$ represents the average size of the $TiO_2$ NPs determined from the particle size distribution.)

Japan) operated at ~200 kV. The nitrogen adsorption and desorption isotherms were measured using a surface area and porosimetry analyzer (Micrometrics, ASAP 2020, USA). The pore volume was measured at the single point $P/P_0 = 0.29$, where $P_0$ represents the equilibrium pressure as the vapor pressure on the sample and P the saturation pressure as the vapor pressure on the liquid.

### 2.3. Evaluation of the photocatalytic reactivity of $TiO_2$ NPs

Methylene blue (MB) was used as an organic solution to evaluate the photocatalytic reactivity of the solid and porous $TiO_2$ NPs fabricated in this study. The light absorbance of the MB solution was evaluated using a UV–Vis spectroscopy. UV and visible absorption spectra were recorded using a UV–visible-near IR spectrophotometer (V-570, JASCO). The transmittance signal was collected at a wavelength ranging from 190 to 2500 nm with a resolution of 0.5 nm. The photocatalytic reactivity was examined using a Pyrex photoreactor with a diameter of 25 cm and an effective volume of 1 L, which was irradiated by a UV lamp (6 W, 320–400 nm) under inner irradiation conditions. For the measurements, the $TiO_2$ NPs (200 mg) were dispersed in a mixed solution of water (960 ml) and MB (40 ml). The resulting solution was magnetically stirred throughout the experiment to homogeneously disperse the $TiO_2$ NPs. The UV irradiation experiments were performed in a dark room to minimize the decrease of MB concentration by unexpected indoor light absorption. After a specific UV irradiation duration, 5 ml of the $TiO_2$ NP-dispersed MB aqueous solution was sampled at regular intervals. Each sample was filtered using a 0.2 μm syringe (polytetrafluoethylene, SH13P020N) to obtain a pure solution (without $TiO_2$) in order to measure the MB concentration.

## 3. Results and discussion

Thermogravimetric analysis (TGA) was carried out to determine the thermal removal temperature of the Brij-58 templates from the $TiO_2$/Brij-58 composite. The TGA results show the weight loss of the samples as a function of the temperature (Fig. 2). The initial weight loss (at less than 150 °C) was triggered by the evaporation of water and organic residues. Then, a steep decrease in both TGA curves was observed at 200–550 °C, which was due to the thermal removal of the Brij-58 templates. Above 550 °C, no weight loss was detected in the samples. The mass ratio of $TiO_2$ to Brij-58/$TiO_2$ was estimated to be approximately 0.42 ($M_{TiO2}$ = 79.866 g·mol$^{-1}$; $M_{TiO2+Brij-58}$ = 192.266 g·mol$^{-1}$), while the molar ratio of $TiO_2$ to Brij-58 was 1:0.1. From this calculation, we expected to obtain the remaining $TiO_2$ content in the Brij-58/$TiO_2$ mixture with a weight change of about 42% after calcination at 550 °C. This was confirmed by the TGA measurements (Fig. 2). Therefore, the calcination temperature was maintained at 550 °C throughout this study in order to thermally remove the Brij-58 templates.

A series of SEM measurements were performed to observe the size and morphology of the synthesized $TiO_2$ NPs while varying the Brij-58 surfactant concentrations (Fig. 3). Hydrolysis and condensation reactions of the $TiO_2$ precursor solution were observed in the aerosolized droplets. Simultaneously, the Brij-58 surfactant molecules supported the pore structures inside the $TiO_2$ NP-based matrix. The increase in the amount of Brij-58 in the $TiO_2$ precursor solution gave no significant change in the resulting structures of the $TiO_2$ NPs fabricated through the aero-sol-gel chemistry process with a subsequent calcination (Fig. 3a–d).

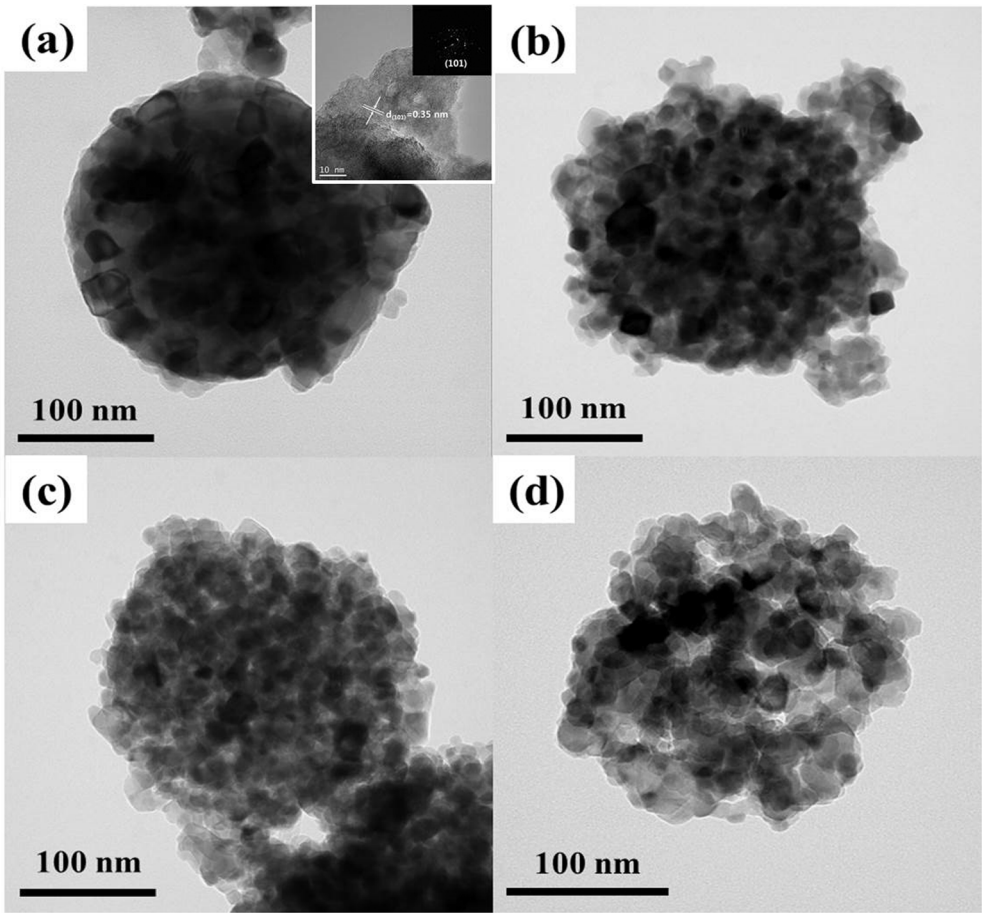


**Fig. 4.** TEM images of (a) solid $TiO_2$ NPs (TNBT:Brij-58 = 1:0.00) (The inset is SAED analysis result), and porous $TiO_2$ NPs: (b) TNBT:Brij-58 = 1:0.01, (c) TNBT:Brij-58 = 1:0.05, (d) TNBT:Brij-58 = 1:0.10.

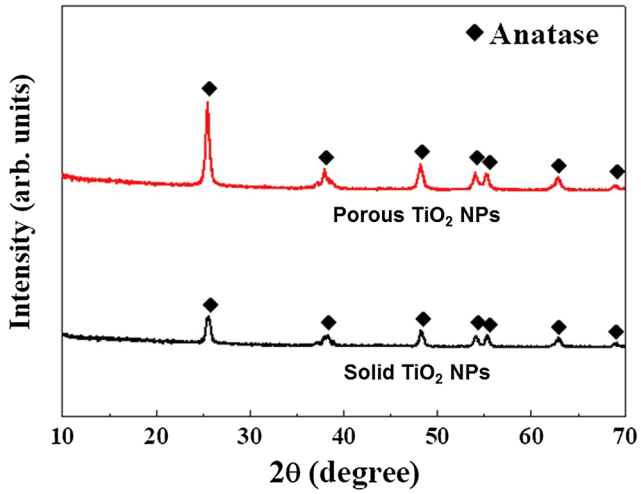


**Fig. 5.** XRD pattern measurements of solid $TiO_2$ NPs (TNBT:Brij-58 = 1:0.01) and porous $TiO_2$ NPs (TNBT:Brij-58 = 1:0.01).

The $TiO_2$ NPs were found to be commonly spherical with a similar average size of ~180 nm (Fig. 3). This suggests that the addition of the Brij-58 surfactant in the $TiO_2$ matrix did not have a significant effect on the overall morphology of the resulting $TiO_2$ NPs. Moreover, it was observed that the surface of the $TiO_2$ NPs formed without Brij-58 (Fig. 3a) was relatively smooth. In contrast, the porous $TiO_2$ NPs formed in the presence of Brij-58 (Fig. 3b–d) were slightly rough. This suggests that the Brij-58 surfactants were dispersed all over the $TiO_2$ matrix and their thermal removal presumably led to the formation of small spaces at the outer surface and inner matrix of $TiO_2$.

The formation of porous structures in the $TiO_2$ NPs fabricated in the present study was corroborated by TEM analysis (Fig. 4). The measurements showed that the small, primary solid $TiO_2$ spheres, formed by the sol-gel process in the aerosolized droplets, were clustered in a large spherical particle due to the fast solvent evaporation (Fig. 4a). As the results of selected area electron diffraction (SAED) analysis shown in the inset of Fig. 4a, the $TiO_2$ NP formed in this study was anatase phase (1 0 1). Also, slight decrease in the electron beam attenuation was observed in the interior of the resulting $TiO_2$ NPs after surfactant removal. This confirmed that the Brij-58 surfactant was present within the interior of the $TiO_2$ NPs (Fig. 4b–d). It should be noted that we also performed elemental mapping analysis using a scanning TEM for the $TiO_2$ NPs fabricated. The weight percent of Ti, O, and C element was found to be 62.51 wt%, 34.07 wt%, and 3.42 wt%, respectively, indicating that the residue of Brij-58 surfactant was remained in the $TiO_2$ matrix with negligibly small amount. As the amount of Brij-58 added to the $TiO_2$ matrix increased, the size of the pores in the $TiO_2$ NPs increased. Since the Brij-58 surfactant molecules were arranged into micelles in the $TiO_2$ precursor solution, they must have acted as templates inside the $TiO_2$ matrix. After these micelles were thermally removed during the calcination process, inner pores were created in the $TiO_2$ matrix. This suggests that the Brij-58 surfactant-templated aerosol process is an easy and versatile method to control the structure of the $TiO_2$ NPs in terms of porosity.

To examine the phase of $TiO_2$ particles formed, XRD analysis was performed for the solid and porous $TiO_2$ NPs fabricated after calcination process at 550 °C. As shown in Fig. 5, strong peaks were observed for a

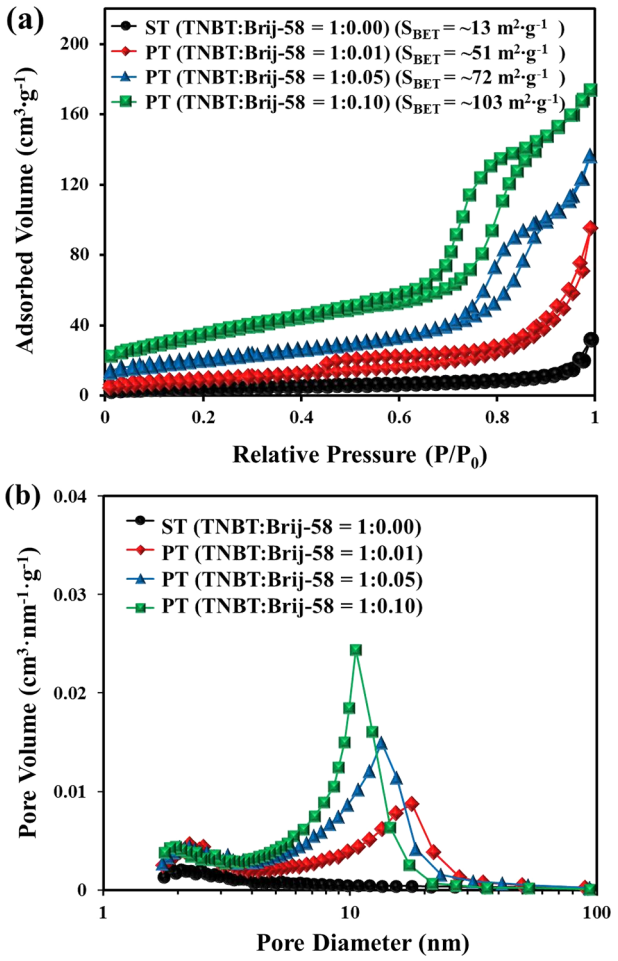


**Fig. 6.** (a) Nitrogen adsorption and desorption of solid and porous $TiO_2$ NPs, (b) pore size distribution of solid and porous $TiO_2$ NPs at various mixing ratios of TNBT and Brij-58. (ST = solid $TiO_2$ NPs, PT = porous $TiO_2$ NPs).

crystal structure with (1 0 1), (0 0 4), (2 0 0), and (1 0 5) in all samples, suggesting that anatase phase was present. This also corroborates the presence of anatase phase of $TiO_2$ detected by using selected area electron diffraction in TEM analysis (Fig. 4a).

The specific surface area and pore volume distribution of the fabricated solid and porous $TiO_2$ NPs were examined using $N_2$ adsorption and desorption isotherms (Fig. 6). A hysteresis loop was observed with a stepwise adsorption and desorption branch at a wide pressure range ($P/P_0$) (Fig. 6a). Solid $TiO_2$ NPs were found to have a specific surface area (SSA) of only ~13 $m^2 \cdot g^{-1}$. In contrast, the presence of Brij-58 in the mixture increased the SSA of the NPS. For porous $TiO_2$ NPs fabricated in the presence of a small amount of surfactant, TNBT:Brij-58 = 1:0.01, the SSA was found to increase to ~51 $m^2 \cdot g^{-1}$. When the amount of Brij-58 in the $TiO_2$ matrix was increased, TNBT:Brij-58 = 1:0.05, the resulting SSA of the porous $TiO_2$ NPs also increased (~72 $m^2 \cdot g^{-1}$). Similarly, the further rise in surfactant concentration, TNBT:Brij-58 = 1:0.10, led to an SSA of ~103 $m^2 \cdot g^{-1}$. The fact that the pore size distribution ranged from several nm to several tens of nm suggested that mesoporous $TiO_2$ NPs were successfully formed through this approach. Moreover, the mesoporous $TiO_2$ NPs were precisely controlled by using the Brij-58 surfactant as a template in the aero-sol-gel process. Investigation of the pore size distribution showed that the solid $TiO_2$ NPs have a pore volume of ~ 0.049 $cm^3 \cdot nm^{-1} \cdot g^{-1}$ (Fig. 6b). In contrast, the pore volume of the porous $TiO_2$ NPs was larger (~0.181 $cm^3 \cdot nm^{-1} \cdot g^{-1}$ for TNBT:Brij-58 = 1:0.01) and showed an increase with the rise in surfactant concentration (~0.226 $cm^3 \cdot nm^{-1} \cdot g^{-1}$ for TNBT:Brij-58 = 1:0.05, and ~0.254 $cm^3 \cdot nm^{-1} \cdot g^{-1}$ for TNBT:Brij-58 = 1:0.10). This suggests that the addition of more Brij-58 in the $TiO_2$ matrix could effectively lead to larger pore structures after thermal removal of the surfactant.

In order to examine the effect of porosity of $TiO_2$ NPs on the MB removal efficiency, a series of experiments for decoloring MB solution under UV light were performed. The MB was degraded by solid and porous $TiO_2$ NPs that were fabricated in the presence of different concentrations of Brij-58 surfactant. The solid and porous $TiO_2$ NPs were added to a MB solution in order to test their photocatalytic reactivity under UV light irradiation. The relative concentration of MB was measured as a function of the UV light exposure duration (Fig. 7a-d). As the UV light exposure duration increased, the dark blue color of original MB solution was turned into light blue (Fig. 7e). The photodegradation of MB using solid and porous $TiO_2$ NPs was investigated by displaying the linear plots of $\ln(C/C_0)$ as a function of the UV irradiation duration (Fig. 7f), where $C_0$ and C represent MB concentration at initial and any time, respectively. All plots were presented as first-order reaction kinetics, and the reaction rate constant ($k$) was calculated from the rate equation $\ln(C/C_0) = kt$, which can be used as an indication of the photocatalytic reactivity [38]. The values of $k$ obtained from the slopes of the linear curves were found to be ~0.164 $h^{-1}$ for solid $TiO_2$ (TNBT:Brij-58 = 1:0.00), ~0.206 $h^{-1}$ for porous $TiO_2$ with TNBT:Brij-58 = 1:0.01, ~0.219 $h^{-1}$ for porous $TiO_2$ with TNBT:Brij-58 = 1:0.05, and ~0.242 $h^{-1}$ for porous $TiO_2$ with TNBT:Brij-58 = 1:0.10. This suggests that the highly porous $TiO_2$ NPs were much more effective in photodegrading MB and had a faster reaction rate. The chemical decomposition of the MB solution occurred through Eq. (1).

$$\text{Dye} + {}^{\cdot}\text{OH} \rightarrow CO_2 + H_2O \quad (1)$$

In other words, the chemical decomposition through the formation of hydroxyl radicals caused weakening of the color. Therefore, the $TiO_2$ photocatalysts accelerated the decomposition of MB through a photochemical process during the UV irradiation. The low reactivity of solid $TiO_2$ was attributed to the poor adsorption of MB molecules due to their low specific surface area. Conversely, the MB removal efficiency was significantly increased when the porosity of the $TiO_2$ NPs was higher. This suggests that the chemical decomposition was accelerated by porous $TiO_2$ because of the large amount of radical oxidation that was formed by the increased pore structures in the $TiO_2$ matrix. Therefore, the removal efficiency of various aquatic pollutants can be potentially improved by employing highly porous $TiO_2$ NPs with excellent photocatalytic reactivity.

## 4. Conclusions

Herein, we demonstrated the formation of solid and porous $TiO_2$ NPs using Brij-58 surfactant-templated aerosol process and a subsequent calcination. The Brij-58 surfactant was employed as a templating medium to support the pore structures inside the $TiO_2$ matrix. After tuning the porosity of the $TiO_2$ NPs by varying the amount of Brij-58 surfactant in the solution, the ability of the mesoporous $TiO_2$ NPs to decompose MB solution under UV light was systematically investigated. It was found that highly porous $TiO_2$ NPs with larger specific surface area and pore volume exhibit faster photocatalytic degradation rates. This suggests that the surfactant-templated aerosol process with subsequent calcination employed in this study is a relatively easy and versatile method to generate highly porous $TiO_2$ NPs. Moreover, the NPs fabricated following this strategy are more effective and highly promising photocatalysts than normal solid $TiO_2$ NPs.

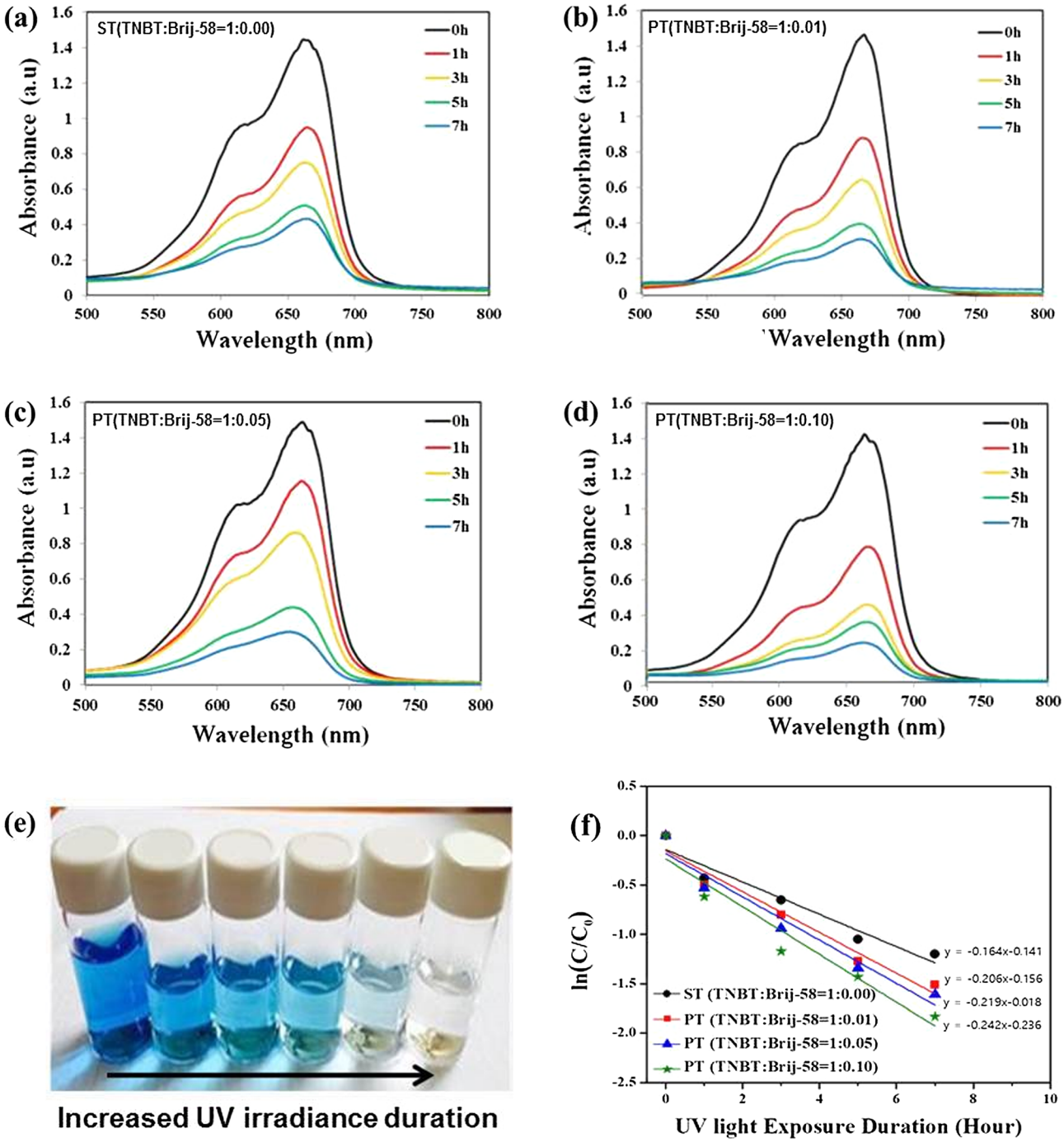


**Fig. 7.** Evolution of light absorbance of MB solution decomposed by (a) solid $TiO_2$ NPs and porous $TiO_2$ NPs: (b) TNBT:Brij-58 = 1:0.01, (c) TNBT:Brij-58 = 1:0.05, (d) TNBT:Brij-58 = 1:0.10 under various UV light exposure duration. (e) The color change of MB solution decomposed by solid $TiO_2$ NPs under UV irradiance. (f) First-order reaction kinetics plots for the photodegradation of MB solution by solid and porous $TiO_2$ NPs in terms of $\ln(C/C_0)$ as a function of UV light exposure duration. (ST = solid $TiO_2$ NPs, PT = porous $TiO_2$ NPs).

## 5. Notes

The authors declare no competing financial interest.

## Acknowledgment

This research was supported by the National Research Foundation of Korea (NRF) grant funded by the Korean Government (Ministry of Science and ICT, MSIT) (No. 2015R1A2A1A15054036 & 2013M3C1A9055407).

## References

[1] A.L. Bolden, C.F. Kwiatkowski, T. Colborn, Environ. Sci. Technol. 49 (2015) 5261–5276.
[2] J. Mo, Y. Zhang, Q. Xu, J.J. Lamson, R. Zhao, Atmos. Environ. 43 (2009) 2229–2246.
[3] X. Zhou, J. Wu, Q. Li, Y. Qi, Z. Ji, P. He, X. Qi, P. Sheng, Q. Li, J. Ren, Chem. Eng. J. 330 (2017) 294–308.
[4] J. Hirayama, Y. Kamiya, ACS Catal. 4 (2014) 2207–2215.
[5] A.L. Linsebigler, G. Lu, J.T. Yates Jr, Chem. Rev. 95 (1995) 735–758.
[6] H. Chen, C.E. Nanayakkara, V.H. Grassian, Chem. Rev. 112 (2012) 5919–5948.
[7] J. Zhang, X. Wang, J. Wang, J. Wang, Z. Ji, Chem. Phys. Lett. 643 (2016) 53–60.
[8] Z.-C. Wu, Y. Lu, Y. Wang, Y.-Z. Li, L. He, X. Cheng, W. Geng, J. Ying, G.-G. Chang,

Chem. Phys. Lett. 708 (2018) 32–36.
[9] S. Costacurta, G.D. Maso, R. Gallo, M. Guglielmi, G. Brusatin, P. Falcaro, ACS Appl. Mater. Interfaces 2 (2010) 1294–1298.
[10] S.H. Lee, M. Kang, S.M. Cho, G.Y. Han, B.W. Kim, K.J. Yoon, C.H.J. Chung, Photochem. Photobio. A 146 (2001) 121–128.
[11] W. Fang, F. Dappozze, C. Guillard, Y. Zhou, M. Xing, S. Mishra, S. Daniele, J. Zhang, J. Phys. Chem. C 121 (2017) 17068–17076.
[12] W.H. Ryu, C.J. Park, H.S. Kwon, J. Nanosci. Nanotechnol. 8 (2008) 5467–5470.
[13] Z. Ding, X. Hu, G.Q. Lu, P.L. Yue, P.F. Greenfield, Langmuir 16 (2000) 6216–6222.
[14] F. Xu, J. Zhang, B. Zhu, J. Yu, J. Xu, Appl. Catal. B: Environ. 230 (2018) 194–202.
[15] F. Xu, L. Zhang, B. Cheng, J. Yu, ACS Sustain. Chem. Eng. 6 (2018) 12291–12298.
[16] A. Meng, S. Wu, B. Cheng, J. Yu, J.J. Xu, Mater. Chem. A 6 (2018) 4729–4736.
[17] A.V. Murugan, V. Samuel, V. Ravi, Mater. Lett. 60 (2006) 479–480.
[18] S. Liu, H. Zhang, M.T. Swihart, Nanotechnology 20 (2009) 235603.
[19] M.D. Blešić, Z.V. Šaponjić, J.M. Nedeljković, D.P. Uskoković, Mater. Lett. 54 (2002) 298–302.
[20] M. Ibadurrohman, K. Hellgardt, ACS Appl. Mater. Interfaces. 7 (2015) 9088–9097.
[21] S.H. Kim, B.Y.H. Liu, M.R. Zachariah, Langmuir 20 (2004) 2523–2526.
[22] S.H. Kim, B.Y.H. Liu, M.R. Zachariah, Chem. Mater. 14 (2002) 2889–2899.
[23] T.J. Liu, Q. Wang, P. Jiang, RSC Adv. 3 (2013) 12662–12670.
[24] C.K. Tsung, J. Fan, N. Zheng, Q. Shi, A.J. Forman, J. Wang, G.D. Stucky, Angew. Chem. Int. Ed. 47 (45) (2008) 8682–8686.
[25] W. Yue, C. Randorn, P.S. Attidekou, Z. Su, J.T. Irvine, W. Zhou, Adv. Funct. Mater. 19 (17) (2009) 2826–2833.
[26] M.F. Atitar, A.A. Ismail, S.A. Al-Sayari, D. Bahnemann, D. Afanasev, A.V. Emeline, Chem. Eng. J. 264 (2015) 417–424.
[27] S. Illa, R. Boppella, S.V. Manorama, P. Basak, J. Phys. Chem. C. 120 (32) (2016) 18028–18038.
[28] J.H. Pan, Z. Cai, Y. Yu, X.S. Zhao, J. Mater. Chem. 21 (2001) 11430–11438.
[29] Y. Zhang, G. Li, Y. Wu, Y. Luo, L. Zhang, J. Phys. Chem. B 109 (2005) 5478–5481.
[30] Z. Xing, W. Zhou, F. Du, L. Zhang, Z. Li, H. Zhang, W. Li, ACS Appl. Mater. Interfaces 6 (2014) 16653–16660.
[31] F. Di Fonzo, C.S. Casari, V. Russo, M.F. Brunella, A.L. Bassi, C.E. Bottani, Nanotechnology 20 (2008) 015604.
[32] Z.R. Ismagilov, L.T. Tsikoza, N.V.E. Shikina, V.F. Zarytova, V.V. Zinoviev, S.N. Zagrebelnyi, Russ. Chem. Rev. 78 (2009) 873.
[33] Y. Ou, J. Lin, S. Fang, D. Liao, Catal. Commun. 8 (2007) 936–940.
[34] E.O. Oseghe, S. Maddila, P.G. Ndungu, S.B. Jonnalagadda, Appl. Catal. B: Environ. 176 (2015) 288–297.
[35] P.S. Shinde, M.A. Mahadik, S.Y. Lee, J. Ryu, S.H. Choi, J.S. Jang, Chem. Eng. J. 320 (2017) 81–92.
[36] G. Calleja, D.P. Serrano, R. Sanz, P. Pizarro, A. García, Ind. Eng. Chem. Res. 43 (2004) 2485–2492.
[37] E.M. Samsudin, S.B.A. Hamid, J.C. Juan, W.J. Basirun, Appl. Surf. Sci. 355 (2015) 959–968.
[38] I.K. Konstantinou, T.A. Albanis, Appl. Catal. B: Environ. 49 (2004) 1–14.